



EUROfusion

EUROFUSION WPJET1-CP(16) 15339

Y.-S. Na et al.

On Benchmarking of Particle Transport Simulations in ITER

Preprint of Paper to be submitted for publication in
Proceedings of 26th IAEA Fusion Energy Conference



This work has been carried out within the framework of the EUROfusion Consortium and has received funding from the Euratom research and training programme 2014-2018 under grant agreement No 633053. The views and opinions expressed herein do not necessarily reflect those of the European Commission.

This document is intended for publication in the open literature. It is made available on the clear understanding that it may not be further circulated and extracts or references may not be published prior to publication of the original when applicable, or without the consent of the Publications Officer, EUROfusion Programme Management Unit, Culham Science Centre, Abingdon, Oxon, OX14 3DB, UK or e-mail Publications.Officer@euro-fusion.org

Enquiries about Copyright and reproduction should be addressed to the Publications Officer, EUROfusion Programme Management Unit, Culham Science Centre, Abingdon, Oxon, OX14 3DB, UK or e-mail Publications.Officer@euro-fusion.org

The contents of this preprint and all other EUROfusion Preprints, Reports and Conference Papers are available to view online free at <http://www.euro-fusionscipub.org>. This site has full search facilities and e-mail alert options. In the JET specific papers the diagrams contained within the PDFs on this site are hyperlinked

On Benchmarking of Simulations of Particle Transport in ITER

Yong-Su Na¹, C.E. Kessel², F. Koechl³, A.R. Polevoi⁴, D. H. Na¹, A. Fukuyama⁵, J. Garcia⁶, N. Hayashi⁷, K. Kim^{1,8}, T. Luce⁹, A. Pankin¹⁰, J.M. Park⁸, F. Poli², A.C.C. Sips¹¹, P. Strand¹², I. Voitsekhovitch¹³, A. Wisitsorasak¹⁴, X. Yuan², and the ITPA Topical Group on Integrated Operation Scenarios

¹Seoul National University, Seoul, Korea

²Princeton Plasma Physics Laboratory, Princeton, New Jersey, USA

³Atominstytut, TU Wien, Fusion@ÖAW, 1020 Vienna, Austria

⁴ITER Organization, Route de Vinon-sur-Verdon, CS 90 046, 13067 St. Paul Lez Durance Cedex, France,

⁵Kyoto University, Kyoto, Japan

⁶Association Euratom-CEA/Cadarache, Saint-Paul-Lez Durance, France

⁷National Institute for Quantum and Radiological Science and Technology, Naka, Ibaraki, Japan

⁸Oak Ridge National Laboratory, Oak Ridge, Tennessee, USA

⁹General Atomics, San Diego, California, USA

¹⁰TECH-X, Boulder, Colorado, USA

¹¹JET Exploitation Unit, Culham Science Centre, Abingdon OX14 3DB, UK

¹²Earth and Space Sciences, Chalmers University of Technology, Sweden

¹³EUROfusion, Garching, Germany

¹⁴King Mongkut's University of Technology Thonburi, Bangkok, Thailand

E-mail contact of main author: ysna@snu.ac.kr

Abstract. We report present status and main results of the ITPA IOS Topical Group activity on the benchmarking of simulations of the core particle transport in ITER baseline ELMy H-mode scenario. The ITPA IOS group is pursuing particle transport as an important component of integrated modelling, because the simulations have shown that dynamics of the particle transport plays a key role in the possibility to access and sustain the H-mode and stable burn conditions and to provide controllable shut-down of DT discharge in ITER. Optimisation of the fuelling scenario for ITER requires sufficiently accurate numerical solvers with appropriate description of particle sources, sinks, boundary conditions and integration in the codes for simulations of self-consistent plasma evolutions. Benchmarking within the ITPA IOS group with various integrated modelling codes is pursued to verify agreement between various integrated modelling codes for specified inputs approximating the expected scenario on ITER. The goal of the benchmark is to compare the sensitivity of particle transport predictions to modelling assumptions and to identify the approaches, which properly address the particle transport issues at different phases of the ITER plasma evolution so to predict ITER plasmas more accurately and to address the critical issues of ITER. It includes comparison of the particle transport solvers, description of the sources and sinks, as well as their implementation in the integrated codes. At the first phase of benchmarking described here we address the particle transport effects related to stationary phase of operation. Firstly, the benchmark is carried out with identical prescribed particle sources, sinks, transport coefficients, and boundary conditions for one time slice in the flat-top H-mode phase. The differences between the codes are identified. The transformation of the particle transport equation is introduced to make possible a direct comparison of the ion solvers and the electron solvers so that their results can be directly compared. Secondly, the pellet fuelling models are benchmarked in various conditions to evaluate the dependency of the pellet deposition profile on the pellet volume, the injection side, the pedestal parameters, and the separatrix parameters.

1. Introduction

The time evolution of the D-T fuel profile in the plasma core has a strong impact on the fusion plasma performance in a fusion reactor. There are several important issues in particle transport on ITER that need to be addressed [1]. The complexity of gas fuelling and core fuelling in different

parts of the discharge poses a question as to how the density is established in L-mode, how it affects the L-H transition, and ultimately how it is controlled in flattop H-mode [2-4]. Particularly, the density profile evolution at the L-H transition has significant implications for entering and staying in H-mode depending on the ratio of the power flux to the SOL to the L-H threshold, P_{sol}/P_{LH} [5]. Developing credible burn control strategies for the H-mode in the flattop phase depends sensitively on the particle balance of the mixed D-T fuels, He and impurities. Other features like the recycling and penetration of He and fuel into the core plasma are central to understanding the dilution and tritium burnup. Ultimately the SOL/divertor plasma and its interactions with plasma facing components will set the boundary conditions for the core transport, and its connections need to be understood. To address these issues, 1.5-D particle transport modelling is essential with integrated transport codes. Although progress has been made in predictive particle transport modelling of the core plasma, and in the area of 2-D SOL/divertor modelling, it is still a much less mature area compared to energy transport. Particle transport in the core plasma is often not treated despite its importance in integrated scenario simulations due to 1) uncertainties of measurements to determine the separatrix density and the 3-D fuel sources to validate transport models, 2) complexity of multi-species impurity transport, and 3) complicated relationship with the scrape-off layer, divertor, and plasma facing materials. Since it is recognized that the particle transport in ITER will be critical to establishing and sustaining the stable burn conditions, the ITPA IOS group is pursuing particle transport as an important component of integrated modelling, as part of a broader scheme to expand toward impurity, alpha particle, and momentum transport.

Core particle transport code benchmarking is carried out within the ITPA IOS group with various integrated modelling codes used for the ITER scenario simulations as done for heat transport [6]. The purpose of the benchmark is to identify the differences in treatment of particle transport between codes in conditions close to those expected in ITER, and to reveal the relevant critical issues to be clarified in dedicated modelling and experiments on present machines so to predict particle transport more accurately. The core particle transport codes in the integrated codes comprise solvers for ion or electron particle transport with consistent metric and transport coefficients, modules for particle sources from the edge gas puffing and the pellet fuelling, modules for particle sinks with ELMs, interfaces with SOL/divertor transport codes or modules for simulating the edge boundary condition consistent with the heat and particle out-fluxes. The systematic multi-code studies of the impact of all aspects of particle transport treatment on the predictions of ITER plasma performance discussed here were never done before.

At the first phase of benchmarking described here we address the particle transport effects related to stationary phase of operation for plasma parameters expected in the baseline 15 MA ITER scenario in the H-mode phase at the current flattop. The study firstly begins with unification of definitions between particle transport solvers by identifying similarities and differences between them. Secondly, the solvers are benchmarked in a stationary target plasma at fixed equilibrium with prescribed particle transport coefficients, sources, and boundary conditions. The ion transport solvers are benchmarked first, then they are benchmarked with the electron transport solvers by modifying the pinch term to allow direct comparison. Thirdly, pellet fuelling is benchmarked in a stationary plasma with prescribed target plasma profiles and equilibrium by scanning the separatrix and the pedestal parameters. This is to benchmark models and to test the dependence of the deposition depth on the pellet volume, the injection side (HFS or LFS), the pedestal and the boundary values. In section 2, we compare the equations used in particle transport solvers and setup of the task for the solvers benchmarking. We compare the results of

simulations for the ion and electron solvers, as well as the sensitivity studies of pellet fuelling predictions for prescribed target plasma parameters in section 3. The discussion and conclusions are summarised in the section 4.

2. Setup for particle transport benchmark study

2.1. Unification of definitions

The particle transport is modelled by the 1-D transport equations for plasma species with diffusion coefficients, pinch velocities, boundary conditions, particle sources and sinks. The particle transport equations are compared as below for unification of definitions between transport codes involved in this benchmarking study where the differences are highlighted in bold red in equations (1)-(5).

ASTRA v.7.0 [7] and ETS [8], the ion/electron particle transport solvers ($k = e, i$) and TRANSP/PTSOLVER [9], the electron particle transport solver ($k = e$)

$$\frac{1}{V'} \left(\frac{\partial}{\partial t} - \frac{1}{2\Phi_{lim}} \frac{d\Phi_{lim}}{dt} \frac{\partial}{\partial \rho} \right) (V' n_k) + \frac{1}{V'} \frac{\partial}{\partial \rho} [V' \langle (\nabla \rho)^2 \rangle] \left(-D_k \frac{\partial n_k}{\partial \rho} + n_k v_k \right) = S_k \quad (1)$$

CRONOS [10], the electron particle transport solver

$$\frac{1}{V'} \frac{\partial}{\partial t} (V' n_e) + \frac{1}{V'} \frac{\partial}{\partial \rho} [V' \langle (\nabla \rho)^2 \rangle] \left(-D_e \frac{\partial n_e}{\partial \rho} - n_e v_e \right) = S_e \quad (2)$$

FASTRAN [11], the electron particle transport solver

$$\frac{1}{V'} \frac{\partial}{\partial t} (V' n_e) + \frac{1}{V'} \frac{\partial}{\partial \rho} [V' \langle (\nabla \rho)^2 \rangle] \left(-D_e \frac{\partial n_e}{\partial \rho} + n_e v_e \right) = S_e \quad (3)$$

JINTRAC [12], the ion particle transport solver ($k = i$) and TASK/TR [13], the ion/electron particle transport solver ($k = e, i$)

$$\frac{1}{V'} \frac{\partial}{\partial t} (V' n_k) + \frac{1}{V'} \frac{\partial}{\partial \rho} [V' \left(-D_k \frac{\partial n_k}{\partial \rho} \langle (\nabla \rho)^2 \rangle + n_k v_k \langle |\nabla \rho| \rangle \right)] = S_k \quad (4)$$

TOPICS [14], the ion particle transport solver

$$\frac{1}{V'} \frac{\partial}{\partial t} (V' n_i) + \frac{1}{V'} \frac{\partial}{\partial \rho} [V' \left(-D_i \frac{\partial n_i}{\partial \rho} \langle (\nabla \rho)^2 \rangle - n_i v_i \langle |\nabla \rho| \rangle \right)] = S_i \quad (5)$$

The core boundary condition is given as $(\partial n / \partial \rho) = 0$ and the edge boundary condition $n(\rho = a)$ can be prescribed. The differences between codes are identified as i) type of particles; ii) description of the plasma shape and volume evolution; iii) sign of the pinch velocity; iv) metric coefficients, $\langle (\nabla \rho)^2 \rangle$ and $\langle |\nabla \rho| \rangle$ used for diffusive and convective terms; v) fuel density loss term due to fusion reactions which are considered in TASK/TR and TOPICS ion solvers. To deal with the inherent difference between ion and electron transport solvers, we compare ion transport solvers first, then compare them with electron transport solvers by modifying the pinch term of the ion solvers to emulate the electron transport solver in the frame of the ion solvers. One example of the modified pinch term is shown below for transport solvers with the definition of the particle flux of $\Gamma_i = -D_i \frac{\partial n_i}{\partial \rho} \langle (\nabla \rho)^2 \rangle + n_i v_i \langle |\nabla \rho| \rangle$;

$$v_D(\Phi) = v_T(\Phi) = -v_e \frac{n_e \langle (\nabla \rho)^2 \rangle}{n_i \langle |\nabla \rho| \rangle} - \frac{D_e}{n_i} \left(\frac{\partial n_e}{\partial \rho} - \frac{\partial n_i}{\partial \rho} \right) \frac{\langle (\nabla \rho)^2 \rangle}{\langle |\nabla \rho| \rangle} \quad (6)$$

where v_e and D_e are the pinch velocity and diffusivity of electrons, respectively and $n_i = 2n_D$ or $2n_T$ or n_D+n_T . In this way, the electron flux that would be obtained with an electron transport equation with fixed impurities can be calculated with the ion transport solvers. Note that the edge boundary condition in the ion solvers should be also properly adjusted to satisfy the prescribed boundary conditions, $n_e(a)$.

The difference in description of the plasma shape and volume evolution is not important for stationary plasmas, considered here (see equations (1), (2)-(5)). Its effect is going to be investigated in benchmarking for simulations of time-evolving plasmas which is out of scope of this paper. The differences from the sign of the pinch term and the toroidal metric could be handled in each code so to ensure the same setup in simulations for the benchmarking study. The fuel density loss term due to fusion reactions which can affect the results significantly depending on the fusion reaction rate is switched off for this benchmark.

2.2. Setup for simulations

The target plasma is set to be the ITER baseline scenario at the stationary plasma current flattop phase with plasma current of 15 MA and toroidal field at the magnetic axis of 5.3 T. The plasma equilibrium is prescribed and fixed. The impurities are prescribed to have the same profile shape as the electron density with a fixed fraction n_Z/n_e where $n_{Be}/n_e = 0.02$ and $n_{Ar}/n_e = 0.0005$ are assumed. The helium profile is prescribed as $n_{He}(\Phi) = n_0 [1 - (\Phi/\Phi_a)^2]^2$, to reflect the core source where Φ is the toroidal magnetic flux and $n_0 = 0.95 \times 10^{19}/m^3$. The quasi-neutrality is enforced in solving the particle transport. The edge particle source is given as $S(\Phi) = S_0 \exp[15(\Phi - \Phi_a)/\Phi_a]$, where $S_0 = 7.5 \times 10^{20}$ atoms/ m^3/s . The core particle source is prescribed as a ‘‘continuous pellet’’ fuelling model: $S(\Phi) = C \times d^2 \times (\Phi/\Phi_a)^{6.5} \times [1 - (\Phi/\Phi_a)]^{8.5} / \{d^2 + [(\Phi/\Phi_a) - 0.5]^2\}$ where $C = 0.25 \times 10^{24}$ and $d = 0.225$. The neutral beam fuelling is ignored. The particle transport coefficients are prescribed as

$$D_e(\Phi) = D_0 + D_1(\Phi/\Phi_a)^2 \text{ for } \Phi < \Phi_{ped} \quad (7)$$

$$D_e(\Phi) = D_2 \quad \text{for } \Phi \geq \Phi_{ped}$$

$R_0 \times v_e / D_e = V_0 \times (\Phi/\Phi_a)^{1/2}$ for transport solvers with the definition of the particle flux of

$$\Gamma_e = -D_e \frac{\partial n_e}{\partial \rho} \langle (\nabla \rho)^2 \rangle - n_e v_e \langle |\nabla \rho| \rangle$$

where $D_0 = 0.5$ m^2/s , $D_1 = 1.0$ m^2/s , $D_2 = 0.11$ m^2/s , $\Phi_{ped}/\Phi_a = 0.88$, $R_0 = 6.2$ m, $V_0 = 1.385$ and positive sign corresponds the inward pinch.

The edge boundary condition is set to be

$$n_e(a) = 4.6 \times 10^{19} / m^3, \quad (8)$$

which is close to the predictions of the SOLPS simulations of the baseline scenario with $P_{sol} = 100$ MW [15].

3. Benchmark results

3.1. Benchmark of ion particle transport solvers

We start the benchmarking for the ion transport solvers first. The same prescription of transport coefficients and sources for electrons described in section 2.2 are used for ion transport solvers but with different boundary conditions to match the electron boundary condition.

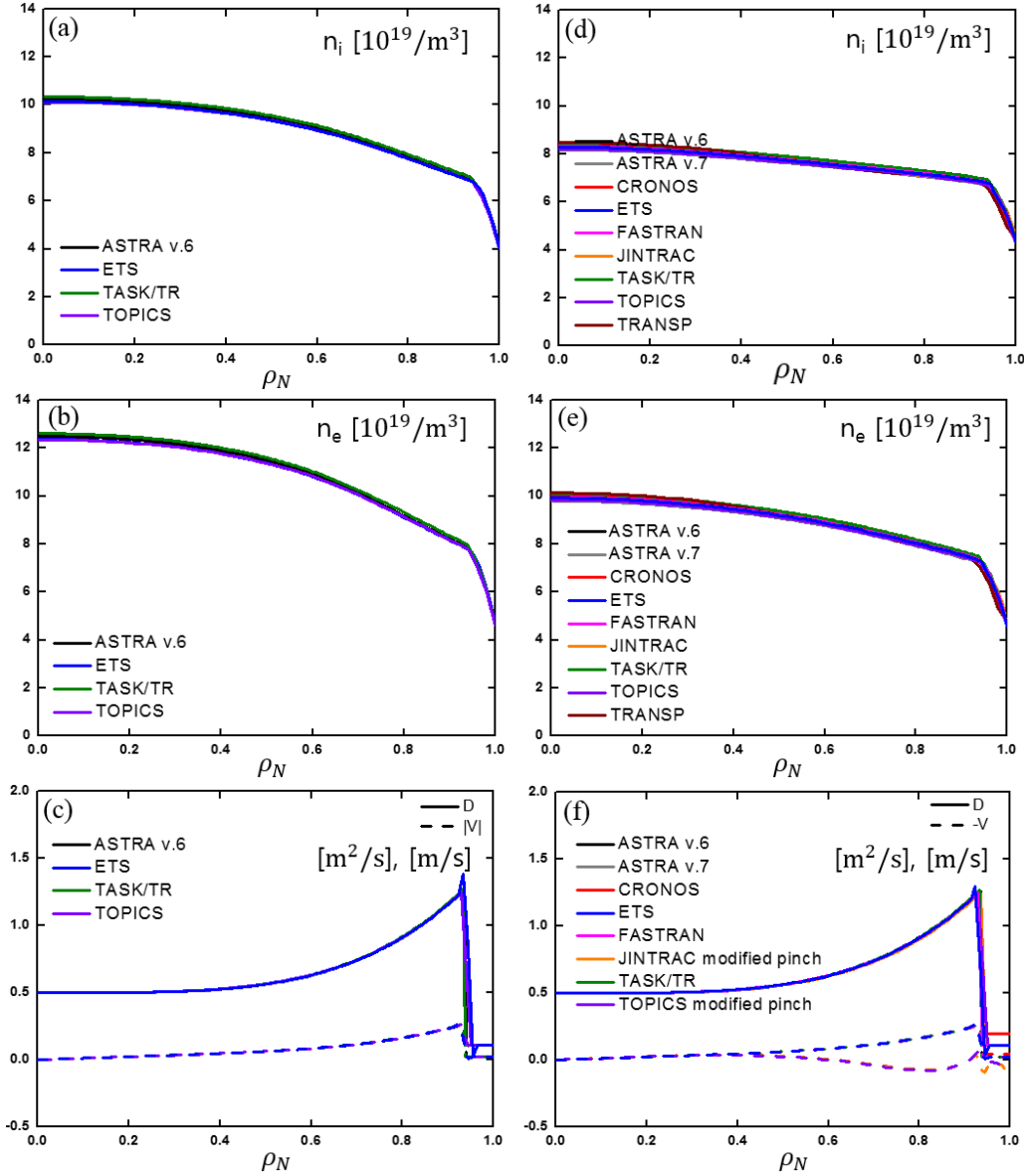


FIG. 1. Particle density profiles predicted from ion (left) and electron (right) transport benchmark for setup of simulations prescribed in section 3.1 and 3.2, respectively. (a),(d) electron density profiles, (b),(e) ion (deuteron+triton+impurity+helium) density profiles, (c),(f) profiles of particle diffusivities and pinch velocities vs. $\rho_N = (\Phi/\Phi_a)^{1/2}$.

Figure 1 (a) and (b) show profiles of the ion density, defined as the sum of deuteron, triton, impurity and helium density and the electron density in $\rho_N = (\Phi/\Phi_a)^{1/2}$ predicted by the various codes. As shown, all the solvers show good agreement within 2%. Some differences come from

difference in equilibrium and grid, confirmed by comparing the enclosed volume in each flux surface, which can affect the number of particle sources, the location of pedestal, the toroidal metric, etc. Note that some codes convert provided input equilibrium data using their own equilibrium solvers.

3.2. Benchmark of electron and transformed ion particle transport solvers

As described in section 2.1, the ion transport solvers can emulate the electron transport solvers by modifying the pinch term. In this section, the ion solvers with these modified pinch terms and the electron solvers are compared based on the guideline described in section 2.2. The profiles of the ion and the electron density and transport coefficients are presented in figure 1 (d)-(f), respectively. The density profiles agree within 3%. Again the differences are originated from the treatment of equilibrium and grid of each solvers.

3.3. Benchmark of pellet fuelling modules

In parallel to the particle transport solver benchmark, we conduct the source model benchmarking. In this paper, we focus on the pellet fuelling because for the baseline scenario the fuelling by gas puffing is expected to be small [4]. To test the dependence of the fuel deposition on the pellet model and on the plasma parameters, we calculate the pellet deposition profile by fixing the equilibrium and profiles of the reference case (ASTRA v.6 in figure 2). The maximal injection speed of the intact pellets for ITER, $v_{\text{pel}} = 300$ m/s is chosen for simulations [4]. A normal injection at the mid-plane is assumed and no edge puffing is applied in the simulations. We evaluate the pellet deposition profiles for i) high field side assumed for plasma fuelling, and low field side injection assumed for ELM pacing by pellets, for ii) small and large pellets with $V_{\text{pel}} = 33 \text{ mm}^3$, the minimal size required for ELM pacing, and 90 mm^3 , the maximal size for pellet in ITER, respectively. We also carried out the sensitivity studies on the pedestal and the separatrix target plasma parameters by varying the pedestal temperature (20% higher and lower than the reference), pedestal density (20% higher and lower than the reference), separatrix temperatures (100% higher and lower than the reference), and separatrix density (20% higher and lower than the reference). For this benchmark study, ASTRA with SMART [16] and JINTRAC with HPI2 [17] are employed for simulating the pellet fuelling. Both models simulate pellet ablation and further drift of ablated particles toward the low field side. The results are presented in figure 2. As shown, JINTRAC with HPI2 predicts deeper deposition of the particles injected with pellet compared to ASTRA with SMART in all cases of the HFS injection. The sensitivity scan of various parameters reveals that the HFS injection provides much deeper particle source due to the LFS drift of the ablated pellet particles toward the plasma centre to the region which is more efficient for fuelling (see figure 2). The large pellets, $V_{\text{pel}} = 90 \text{ mm}^3$ produce about three times higher peaked deposition profile with deeper penetration than small ones, $V_{\text{pel}} = 33 \text{ mm}^3$ as shown in figure 2. The pedestal temperature has stronger impact on the particle deposition than the pedestal density with the HPI2 model. The depth of deposition increases with increase of the pedestal temperature (see figure 2 (c), (d)). The SMART model predictions are much less sensitive to the edge plasma density and temperature variations within the range described above. The separatrix density and the temperature do not affect the deposition profile for the changes enforced in this study. Note that both models predict similar depth of the pellet ablation for each of the pellet size. For 33 and 99 mm^3 LFS and HFS pellets in process of ablation penetrate to the top of pedestal, i.e. sufficiently deep to trigger ELMs. For LFS pellets (figure 2 (b)) the SMART

model predicts almost full removal of ablated particles due to the outward drift even for small pellets, which agrees with the assumptions of integrated analysis [4]. The HPI2 model predicts rather strong residual fuelling from the LFS close to the plasma edge, which can strongly affect the possibility of independent ELM pacing and density control by pellet injection [4]. The increase of the particle flux to the SOL caused by such skinned particle sources can affect control of the divertor detachment. This requires dedicated integrated modelling and further validation of the pellet models in particular for the LFS injection.

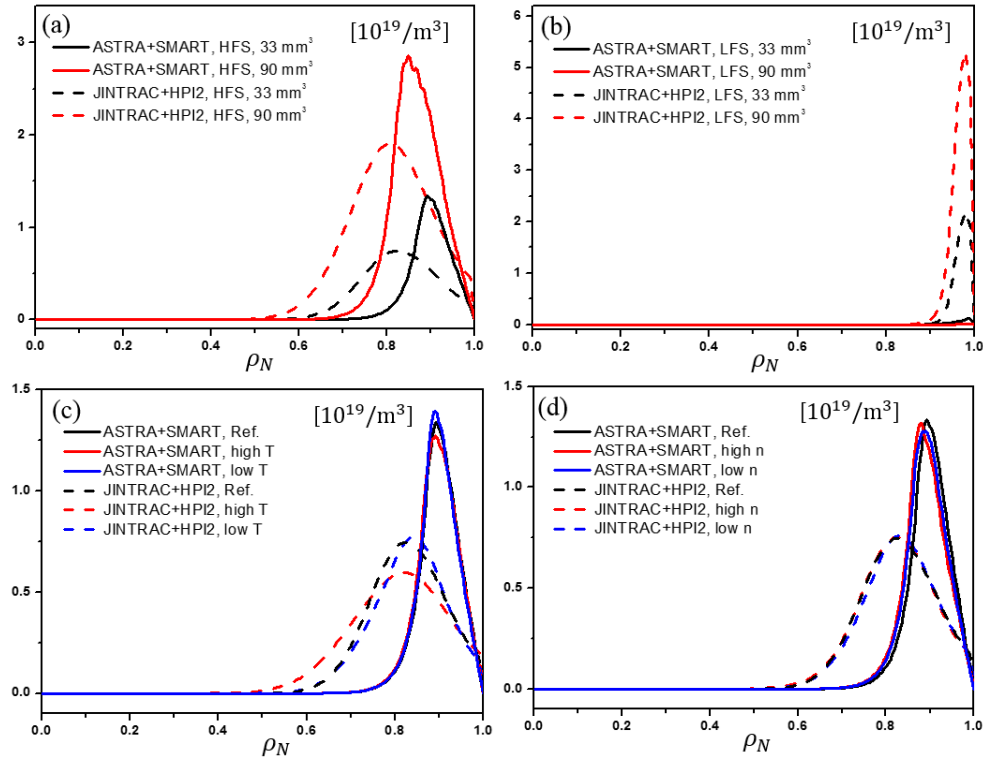


FIG. 2. Particles deposition profiles predicted by ASTRA with SMART (dashed lines) and JINTRAC with HPI2 (solid lines) for (a) HFS injection with pellet volume of 33 mm³ and 90 mm³, (b) LFS injection with pellet volume of 33 mm³ and 90 mm³, (c) various pedestal temperatures, (d) various pedestal densities with HFS injection, $V_{\text{pel}} = 33 \text{ mm}^3$ vs. $\rho_N = (\Phi/\Phi_a)^{1/2}$

4. Discussion and Conclusions

The core particle transport codes are benchmarked with the integrated transport codes used for ITER scenario modelling within ITPA IOS Topical Group. At the first phase, we compared the particle transport solvers for the ions and the electrons with prescribed transport coefficients, stationary sources, and boundary conditions for plasma parameters, expected at a stationary phase of ITER baseline ELMy H-mode scenario. To make possible the benchmarking we identified the differences between particle transport solvers and then unified the definitions. It was found that some of the ion solvers assume different metric coefficients for the diffusive and the convective terms. For such solvers the ratio D/v cannot be directly translated to the density profile peaking or stiffness, $L_n = n/n'$, which makes less trivial the comparison with the experiments. On the other hand, the selection of metric coefficients made with these solvers is the only one for which v corresponds to the flux surface average of the orthogonal local fluxes and for which transport coefficients D and v are invariant with respect to the choice of the flux surface label as detailed in

[7]. We benchmarked the ion transport solvers first. Then the ion solvers were adopted for emulation of the electron transport solvers by modifying the pinch term and benchmarked with the electron solvers. The calculated density agrees within 3% for each step of benchmarking and the difference mainly results from treatment of equilibrium and grid. It is noteworthy that differences of the particle profile predictions are observed between step 1, where the benchmark for ions, and the step 2 where the benchmark for the electrons with the same particle diffusivity and pinch velocity (compare the left and right columns of figure 1). Such big difference is caused by presence of noticeable fraction of helium ash with relatively high peaking, which increases the difference between the fuel and the electron density gradients. For present day machines $n_i' \sim n_e'$, and the difference vanishes to zero (see equation (6)). Thus, such a big difference is the specific feature of the burning plasmas. Therefore, for fusion reactors it is extremely important to use appropriate theory-based transport models to set-up choosing between the solvers for the electron and the ion transport. For empirical and semi empirical particle transport model, the predictive capability becomes more uncertain. Note that the electron density peaking affects the temperature peaking for the stiff models and thus, the fusion power, the fuel ion peaking affects the fusion power directly by $P_{\text{fus}} \sim n_D n_T (\rho=0)$. We also benchmark the pellet fuelling modules. Two pellet fuelling models are benchmarked for prescribed target plasma and pellet injection parameters to reveal the sensitivity of the deposition profiles to the injection side, the pellet volume, the pedestal parameters, and the separatrix parameters. Modelling of the HFS fuelling demonstrates noticeable dependence of the depth of the particle source on the injected pellet size and weak sensitivity to the other parameters for both models. For LHS injection one of the models predicted noticeable residual fuelling which can affect the integrated control of fuelling, ELM mitigation, and divertor detachment. The numerical analyses of such possible impact and dedicated validation of pellet modelling of the LHS pellets is required. The study will be continued for time-evolving plasmas to investigate the role of the plasma shape and volume evolution term and to improve the integrated modelling of time-evolving plasmas. Finally, the impact of the particle transport to fusion performance will be evaluated in ITER.

Disclaimer is present: The views and opinions expressed herein do not necessarily reflect those of the ITER Organization

References

- [1] A.C.C. Sips, et al., Phys. Plasmas 22 021804 (2015)
- [2] A. Loarte, Nucl. Fusion 54 123014 (2014)
- [3] M. Romanelli, et al., Nucl. Fusion 55 (2015) 093008
- [4] A.R. Polevoi, et al., Nucl Fusion 56 (2016) (to be published)
- [5] A. Loarte, et al., Nucl. Fusion 53 083031 (2013)
- [6] C.E. Kessel, et al., Nucl. Fusion 47 1274 (2007)
- [7] G. Pereverzev, et al., IPP-Report IPP 5/98 (2002), E. Fable, IPP-Report (2012)
- [8] D. Kalupin, et al., Nucl. Fusion 53 (2013) 123007
- [9] R.J. Goldston, et al., J. Comput. Phys. 43 61 (1981)
- [10] J. F. Artaud et al., Nucl. Fusion 50, 043001 (2010)
- [11] J.M. Park, et al., Proc. 23rd Int. Conf. on 2010 Fusion Energy (Daejeon, Korea, 2010) (Vienna: IAEA) CD-ROM file EXC/P2-05
- [12] M. Romanelli, et al., Plasma and Fusion Research 9 3403023 (2014)
- [13] M. Honda, et al., Nucl. Fusion 46 580 (2006)
- [14] H. Shirai, et al., Plasma Phys. Control. Fusion 42 1193 (2000)
- [15] H.D. Pacher, et al., J. Nucl. Mater. 463 591 (2015)
- [16] B. Pégourié, et al., Plasma Phys. Contr. Fusion 51 124023 (2009)
- [17] B. Pégourié, et al., Nucl. Fusion 47 44 (2007)